Applied Catalysis B: Environmental 244 (2019) 546–558

Contents lists available at ScienceDirect

Applied Catalysis B: Environmental

journal homepage: www.elsevier.com/locate/apcatb

Silver decorated magnetic nanocomposite (Fe_3O_4@PPy-MAA/Ag) as highly active catalyst towards reduction of 4-nitrophenol and toxic organic dyes

Raghunath Das[a,*], Venkata Satyanarayana Sypu[a], Hugues Kamdem Paumo[a], Madhumita Bhaumik[a], Vinesh Maharaj[b], Arjun Maity[a,c,*]

[a] Department of Applied Chemistry, University of Johannesburg, Johannesburg, South Africa
[b] Department of Chemistry, University of Pretoria, Pretoria, South Africa
[c] DST/CSIR National Centre for Nanostructured Materials, Council for Scientific and Industrial Research, 1-Meiring Naude Road, Pretoria 0001, South Africa

ARTICLE INFO

Keywords:
Ag NPs
Magnetic conducting polymer
4-Nitrophenol
Organic dye degradation
Recyclability

ABSTRACT

Developing innovative technologies for the efficient treatment of wastewater containing toxic organic pollutants is of particular importance worldwide. Removal of organic contaminants from aqueous media through chemical reduction using noble metal-based nanocatalysts, and in the presence of $NaBH_4$, as a reducing agent, has become an established approach in the last few years. Herein, we describe a simple method for the synthesis of a magnetic conducting polymer modified with mercaptoacetic acid (MAA) and silver nanoparticles (Ag NPs) as a promising catalyst for the reduction of organic pollutants. Ag NPs were deposited on the magnetic conducting polymer by the reduction of a silver salt precursor ($AgNO_3$) without the need for a reducing agent or stabilizer. The developed Fe_3O_4@PPy-MAA/Ag nanocomposite was characterised using FE-SEM, TEM, XRD, XPS, BET and ATR-FTIR. The catalytic performance of the nanocatalyst during the reduction of 4-nitrophenol (4-NP) and organic dyes, namely, methylene blue (MB) and methyl orange (MO) was assessed in aqueous medium at 25 °C. The catalyst exhibited excellent catalytic activity for the reduction of all three targeted organic pollutants (4-NP, MO and MB). The pseudo-first-order rate constants were estimated as 0.5–14.3 × 10^{-2} min^{-1}, 0.52–24.2 × 10^{-2} s^{-1} and 10.1–46.8 × 10^{-3} s^{-1} for the reduction of 4-NP, MO and MB, respectively. The magnetic catalyst was separated easily from the reaction medium and recycled without significant loss of catalytic activity up to eight successive cycles. In addition to its green synthesis and reusability, findings from this study show that Fe_3O_4@PPy-MAA/Ag nanocomposite has the potential efficiency and stability to make it an ideal catalyst in environmental applications *via* chemical reduction of toxic contaminants from wastewater.

1. Introduction

While modern industries have grown in leaps and bounds over the past few decades, so far environmental pollution become a global and serious concern to human well-being. Among various types of environmental pollution, contamination of water bodies due to the discharge of untreated water-containing inorganic and organic species has attracted a lot of consideration in recent years [1–4]. In particular, the uncontrolled discharge of azo dyes, commonly used in the leather, textile, plastic, cosmetics, ink, paper, and foodstuff industries, is considered to induce significant damage to aquatic environments [5,6]. Owing to their photo- and thermal stability, as well as their ability to resist biodegradation, organic dyes can persist in the environment for an extended period of time. The presence and persistence of these oxygen-sequestering species in the water systems has been reported to reduce light penetration and thereby inhibits photosynthesis of aquatic vegetation [7,8]. Therefore, it is essential to degrade and decolourize the industrial effluents containing toxic organic dyes before they can be discharged safely to the natural environment. Along with organic azo dyes, phenolic compounds, such as the notable nitrophenol derivatives, are considered by the U.S. EPA as priority pollutants that directly affect the environment and human health [9]. Refractory 4-nitrophenol (4-NP) in water bodies are known to originate from effluents of industries such as petrochemical, pesticides, pharmaceuticals, preservatives, explosives, dyes and wood [10,11]. Hence, as with azo dyes, it is equally important to find effective methods for their removal from industrial wastewater before they can be release into the environment. Catalytic reduction of 4-NP to its amino derivative, 4-aminophenol (4-AP), has drawn much attention in the area of environmental remediation. Amino arenes are well-known for the valuable roles played in pharmaceutical

* Corresponding authors.
E-mail addresses: dasraghunath87@gmail.com (R. Das), amaity@csir.co.za (A. Maity).

https://doi.org/10.1016/j.apcatb.2018.11.073
Received 22 August 2018; Received in revised form 16 November 2018; Accepted 24 November 2018
Available online 26 November 2018
0926-3373/

and photographic applications [12]. 4-AP serves as key intermediate in the synthesis of numerous antipyretic and analgesic medications, whilst in photographic development this compound is used for its strong reducing character. Therefore, the development of materials with high performance for dye degradation, as well as for 4-NP reduction, can be of great significance in reducing environmental pollution.

In recent years, the design and synthesis of nano-sized metals with controlled morphology and texture have been favoured over their bulk counterparts because of their enhanced catalytic, magnetic, electronic and optical properties [13–15]. Notably, noble metal nanoparticles are well-reported for their closely-packed structure, availability of free electrons in the valence band, and high surface area to volume ratio [16]. In particular, the use of relatively low-cost silver nanoparticles (Ag NPs) has been increasingly investigated in applications including catalysis, sensors, cosmetics and disinfecting medical devices, due to their desirable physical and chemical properties [17–19]. Controlled growth, particle size, shape and long-term stability play significant roles in the performance activity of Ag NPs. However, metal nanoparticles having desirable morphological properties as catalysts often suffer drawbacks such as (i) propensity to aggregate, leading to lowered efficiency due to their higher surface energy, (ii) difficult recovery from the reaction medium for reusability due to nanoscale [20,21]. To overcome these drawbacks, innovative approaches to immobilize the metal NPs onto solid supports to engender hybrid nanostructures have been introduced. Such efforts have successfully controlled the growth of particles to specific size ranges during preparation, as well as improving the catalytic activity and stability through synergistic effects [22–24].

Recent research has attempted to further enhance the activity of metal nanoparticles through the use of solid supports like polymers, graphene sheets, metalorganic frameworks (MOF) and metal oxides [25–27]. It is now generally accepted that in addition to their ability to improve catalytic activity, a conducting polymer matrix with controlled shape could provide long-term stability to the metal NPs. Among conducting polymers, polypyrrole (PPy) has attracted substantial consideration because of its high electrical conductivity, good redox properties and ease of preparation [28–30]. Diverse metal based PPy nanocomposites with distinct morphologies like Pt-PPy [28], Ag-PPy coaxial nanocables [31], Au-PPy [32] and Fe_3O_4/PPy/Au [33] have been fabricated for their improved electrocatalytic activity as well as environmental stability. Furthermore, the incorporation of selective chelating ligands into the polypyrrole network has become a promising technology for trapping and stabilizing heavy metal ions. The stability of metal-ligand complex plays a vital role for the selective binding of the metal ions. For example, thiol-containing chelating ligands have high adsorption affinity for silver ions due to the high stability of thiol-silver complex [34,35]. Nevertheless, one key issue in catalysis is the fact that spent catalysts are not always easy to separate from the reaction mixture for use in subsequent reactions. In contrast, magnetic iron oxide nanoparticles (Fe_3O_4) have drawn increasing attention because their superparamagnetic nature allows for easy recovery from reaction medium by applying an external magnetic field [36,37]. Additionally, they also exhibit high stability, dispersion and catalytic efficiency.

The present investigation describe the simple preparation of Ag NPs decorated magnetic polypyrrole composite (Fe_3O_4@PPy-MAA/Ag) *via* a two-step process. In the first step, the modification and magnetization of the PPy matrix is performed by oxidative polymerization of pyrrole in the presence of mercaptoacetic acid (MAA) and iron (II,III) oxide NPs. The next step is the reduction between $AgNO_3$ and the amino/thiol-rich Fe_3O_4@PPy-MAA, and the subsequent deposition of Ag NPs at room temperature under organic solvent-free conditions. The PPy matrix in the Fe_3O_4@PPy-MAA nanocomposite has electron donor groups which act as a reducing agent and stabilizer. The catalytic activity of the as-prepared Fe_3O_4@PPy-MAA/Ag magnetic material was evaluated for the reduction of 4-NP to 4-AP in the presence of a reducing agent ($NaBH_4$). Furthermore, the catalytic efficiency of this novel nanocomposite was also tested in the degradation of harmful dyes, *viz.* methyl orange (MO) and methylene blue (MB) in aqueous media.

2. Materials and methods

2.1. Chemicals

Pyrrole monomer (Py, 99%, Sigma-Aldrich, USA) was purified by vacuum distillation and stored at 4 °C prior to usage. Ammonium persulfate (APS), iron oxide (Fe_3O_4) of 50 to 100 nm particle size, mercaptoacetic acid (thioglycolic acid), silver nitrate and sodium borohydride ($NaBH_4$) were obtained from Sigma-Aldrich (USA). 4-nitrophenol (4-NP), methyl orange (MO), methylene blue (MB), sodium bicarbonate, dichloromethane and acetone were supplied by Sigma-Aldrich (USA). The organic solvents and all other chemicals were used without further purification. Throughout the experiment, double distilled water was used for aqueous solutions preparation.

2.2. Synthesis of Fe_3O_4@PPy-MAA nanocomposite

Magnetic Fe_3O_4 deposited thioglycolic acid modified polypyrrole nanocomposite (Fe_3O_4@PPy-MAA) was prepared according to a previously reported *in situ* oxidative polymerization technique [38]. Initially, 0.2 g Fe_3O_4 nanoparticles were dispersed in 80 mL double distilled water through ultra-sonication for 30 min. Then, 0.8 mL pyrrole followed by 1.6 mL thioglycolic acid was added. The resultant mixture was vigorously shaken for 30 min to ensure a homogeneous mixture. Afterwards, 6.8 g oxidant (APS) was dissolved in 10 mL water and added dropwise with vigorous shaking. The resultant aqueous suspension was allowed to stand at ambient temperature (25 °C) for an additional 5 h to complete the polymerization process. The black precipitation obtained was collected by vacuum filtration, followed by washing 5 times with double distilled water and acetone. This product was dried overnight in a vacuum oven at 60 °C to obtain a constant weight of magnetic Fe_3O_4@PPy-MAA nanocomposite.

2.3. Preparation of silver decorated magnetic nanocomposites (Fe_3O_4@PPy-MAA/Ag)

A batch adsorption technique was used in the preparation of silver decorated magnetic nanocatalysts (Fe_3O_4@PPy-MAA/Ag). The Fe_3O_4@PPy-MAA composite was employed as an effective adsorbent for silver ions in aqueous solution and their subsequent chemical reduction. The presence of electron rich functionalities (−SH, −COOH and −NH) in the polymer matrix plays an important role for the reduction of silver ion (Ag^{+1}) to its metallic state (Ag°). In a typical procedure, a solution of 200 mg/L aqueous silver ions solution was first prepared using $AgNO_3$ salt. Then, a fixed amount of Fe_3O_4@PPy-MAA (0.5 g) was added to 1 L of the prepared silver ion solution. The whole system was kept at 25 °C in a water bath under stirring conditions for 5 h. Finally, the silver adsorbed magnetic composite was filtered, washed with double distilled water, and dried under vacuum at room temperature. The residual silver ion concentration was determined using ICP-MS, and the mass loading of silver onto the Fe_3O_4@PPy-MAA surface was calculated to be 28.3 wt%.

2.4. Characterization techniques

The detailed structural and morphological characteristics of the developed magnetic nanocomposites were analysed using a Field Emission-Scanning Electron Microscope (Auriga FESEM, Carl Zeiss, Germany) with an attached energy dispersive X-ray spectrometer (EDX, Oxford, UK). High Resolution-Transmission Electron microscope (HR-TEM, JEM-2100, JEOL Japan) investigations were performed with a LaB6 filament operated at 200 kV. The chemical functionality of the Fe_3O_4@PPy-MAA and silver loaded catalyst was assessed using

Attenuated Total Reflectance-Fourier Transform Infrared (ATR-FTIR, Perkin-Elmer, USA) spectroscopy. The crystallinity of the metallic silver in the catalyst was determined by a PANalytical (X'Pert PRO) X-ray diffraction (XRD) diffractometer using Cu Kα radiation (wavelength, λ = 1.5406 Å), and angular variation of 5-90° operated at a generator voltage and current of 40 kV and 40 mA, respectively. The specific surface areas of the PPy-MAA, Fe_3O_4@PPy-MAA and Fe_3O_4@PPy-MAA/Ag were determined using the Brunauer-Emmett-Teller (BET) method, based on low temperature N_2 adsorption-desorption technique using a Micromeritics TRISTAR II 3020 BET analyser. Pore size distributions were measured from the adsorption isotherms applying the Barrett-Joyner-Halanda (BJH) method. The magnetic properties of the developed material were measured using vibrating sample magnetometer (VSM) of a physical property measurement system (PPMS) by Quantum Design. The binding energy of the surface phase composition of the magnetic nanocomposites was recorded by X-ray photoelectron spectroscopy (XPS, Kratos, UK) using monochromatic Al Kα radiation. The residual concentration of Ag^+ ions after adsorption procedure onto the surface of the Fe_3O_4@PPy-MAA was determined using an inductively coupled plasma mass spectrometer (ICP-MS) (Thermo Fisher Scientific, USA). UV–vis spectrophotometer (Perkin-Elmer, Lambda 35) was used to measure the concentration of 4-Nitrophenol and organic dyes (methylene blue and methyl orange) in the reaction medium during catalytic processes. A Waters® Synapt G2 high definition mass spectrometry (HDMS) system (Waters Inc., Milford, Massachusetts, USA) was used for compound detection and analysis. The system consists of a Waters Acquity Ultra Performance Liquid Chromatography (UPLC®) for the separation of the compounds hyphenated to the quadrupole-time-of-flight (QTOF) instrument. A Kinetex® 1.7 µm EVO C18 100 Å (2.1 mm ID x 100 mm length) column was used. The mobile phase consisted of solvent A: water with 0.1% formic acid and solvent B: acetonitrile with 0.1% formic acid). The gradient elution was optimized as follows: 3% B (0-0.1 min), 3% B (0.1–7.5 min), 100% B (7.5–9.0 min), 3% B (9.0–10.0 min). The flow rate was 0.4 ml/min, column temperature constant at 40 °C for the entire run, a total run time of 10 min and the injection volume was 5 µl. The instrument was calibrated by direct infusion of 5 nM sodium formate solution at a flow rate of 10 µl/min over a mass range of 50–1200 Da. The following MS source parameter were set for both positive and negative mode: Source temperature 100 °C, sampling cone 15 V, extraction cone 4.0 V, desolvation temperature 400 °C, cone gas flow 10.0 L/h, desolvation gas flow 700 L/h, capillary 2.0 kV. The positive and negative ion mass spectra were collected in separate chromatographic runs (employing the same separation conditions). Compounds were identified based on their accurate mass generated from MassLynx V 4.1, iFit value, MS/MS fragmentations (product ions).

2.5. Catalytic study

2.5.1. Catalytic reduction of p-nitrophenol (4-NP)

The catalytic activity of the Fe_3O_4@PPy-MAA/Ag nanocomposites were tested using the reduction of 4-nitrophenol to 4-aminophenol as a model. In a typical reaction, 2.5 mg Fe_3O_4@PPy-MAA/Ag catalyst was added to 25 mL aqueous solution of 4-NP (1 mmol) under stirring condition at 25 °C in a 50 mL round bottom flask. Next, freshly prepared 2.5 mL aqueous solution of $NaBH_4$ (1×10^{-1} M) was slowly added to the above reaction mixture. A sudden change in colour from light to dark yellow was experienced. The progress of the -NO_2 conversion was monitored by the change in absorbance at the wavelengths of 400 nm for 4-NP and 300 nm for newly formed 4-AP, at definite time intervals. The colour change from dark yellow to colourless happened within 45 min of reaction time. With a fixed concentration and volume of 4-NP and $NaBH_4$, the amount of catalyst was also varied from 2.5 to 7.5 mg, to evaluate the efficiency of the developed Fe_3O_4@PPy-MAA/Ag catalyst. Furthermore, to investigate the catalytic potentiality of Ag NPs, relative to Fe_3O_4 NPs, Both Fe_3O_4@PPy-MAA and Fe_3O_4@PPy-MAA/Ag were equally employed for the same reaction without $NaBH_4$.

2.5.2. Catalytic reduction and degradation of MB and MO dyes

For this study, two water-soluble organic dyes, namely, methyl orange (MO) and methylene blue (MB) were chosen as model for the reduction and degradation using Fe_3O_4@PPy-MAA/Ag in the presence of reducing agent $NaBH_4$. In a typical degradation process, different amounts of the as-prepared Fe_3O_4@PPy-MAA/Ag (1.0–5.0 mg) were added to 25 mL of aqueous dye solution (1×10^{-4} M). Subsequently, 1 mL freshly prepared $NaBH_4$ solution (1×10^{-1} M) was added to the above mixture and the reaction was stirred at 25 °C. The catalytic activity was recorded by using UV–vis absorption spectra (λ_{max}: 464 nm for MO; λ_{max}: 664 nm for MB) of supernatant at selected time intervals. Samples were also analysed using the UPLC-QTOF-MS.

3. Results and discussion

3.1. Characterization

The general morphology and composition of the as-developed magnetic nanocomposites were investigated using FESEM and EDX. A close view of the FE-SEM image of the Fe_3O_4@PPy-MAA (Fig. 1a) revealed a smooth surface morphology covered by an even distribution of nearly spherical particles. After deposition of metallic silver onto the magnetic nanocomposite, Fig. 1b shows larger cluster of aggregated globules with rough surface. The EDX spectra for the surface elemental composition of the synthesized nanocomposites are displayed in Fig. 1c and d. As expected, Fig. 1c shows the presence of carbon, nitrogen, oxygen, sulphur and iron as the major elemental composition of the Fe_3O_4@PPy-MAA composite. Appearance of sharp and intense peak of silver in the EDX spectrum of Fe_3O_4@PPy-MAA/Ag (Fig. 1d), along with C, N, O, S and Fe, clearly indicated that the Ag NPs have been deposited on the surface of the Fe_3O_4@PPy-MAA nanocomposite.

The size, morphology, and structural properties of the prepared material were examined by high resolution transmission electron microscopy (HR-TEM). As shown in Fig. 2a, the TEM image of iron oxide-embedded polypyrrole matrix revealed spherical morphology. However, the surface morphology of the magnetic nanocomposite has been changed after deposition of metallic Ag nanoparticles. Fig. 2b exhibits that the Ag NPs are distributed across the Fe_3O_4@PPy-MAA composite surface and no agglomeration was found throughout the polymer-based matrix. Furthermore, HR-TEM image (Fig. 2c) showed well-defined lattice fringes, which confirmed the crystallinity of the prepared nano materials. The calculated lattice spacing (d-spacing) of 0.23 and 0.49 nm can be ascribed to the (111) fcc lattice plane of the Ag and Fe_3O_4 NPs, respectively [39–41].

In order to examine the chemical changes of the magnetic nanocomposite before and after Ag NPs deposition, FTIR spectra were recorded in the wavenumbers range 4000–600 cm^{-1} (Fig. S1 in supporting information). The presence of broad bands around at 3118 cm^{-1} and 2919 cm^{-1} are ascribed to the fundamental O—H and C–H stretching vibrations, respectively. The weak broad band near the 2635–2445 cm^{-1} region may be attributed to S—H vibrations of thioglycolic acid [42]. The strong characteristic peak close to 1703 cm^{-1} demonstrates vibrations of carboxyl group (C═O) of thioglycolic acid. In addition, the spectra exhibited strong bands at 1555 and 1488 cm^{-1}, attributed to the antisymmetric and symmetric stretching mode of the Py backbone along the polymer chain [43]. The peaks at 1355 and 1275 cm^{-1} are assigned to C–N and C–O stretching frequencies, respectively. The band at 1044 is attributed to C–H deformation vibrations of the ring structure. The intense bands at 1190 and 924 cm^{-1} are typical bands for doped PPy [43]. Therefore, the FTIR spectroscopy study confirmed the successful modification of PPy matrix by thioglycolic acid in Fe_3O_4@PPy-MAA and Fe_3O_4@PPy-MAA/Ag.

To examine the crystalline purity and phases, powder X-ray diffraction (XRD) patterns were carried out for pure Fe_3O_4 nanoparticles,

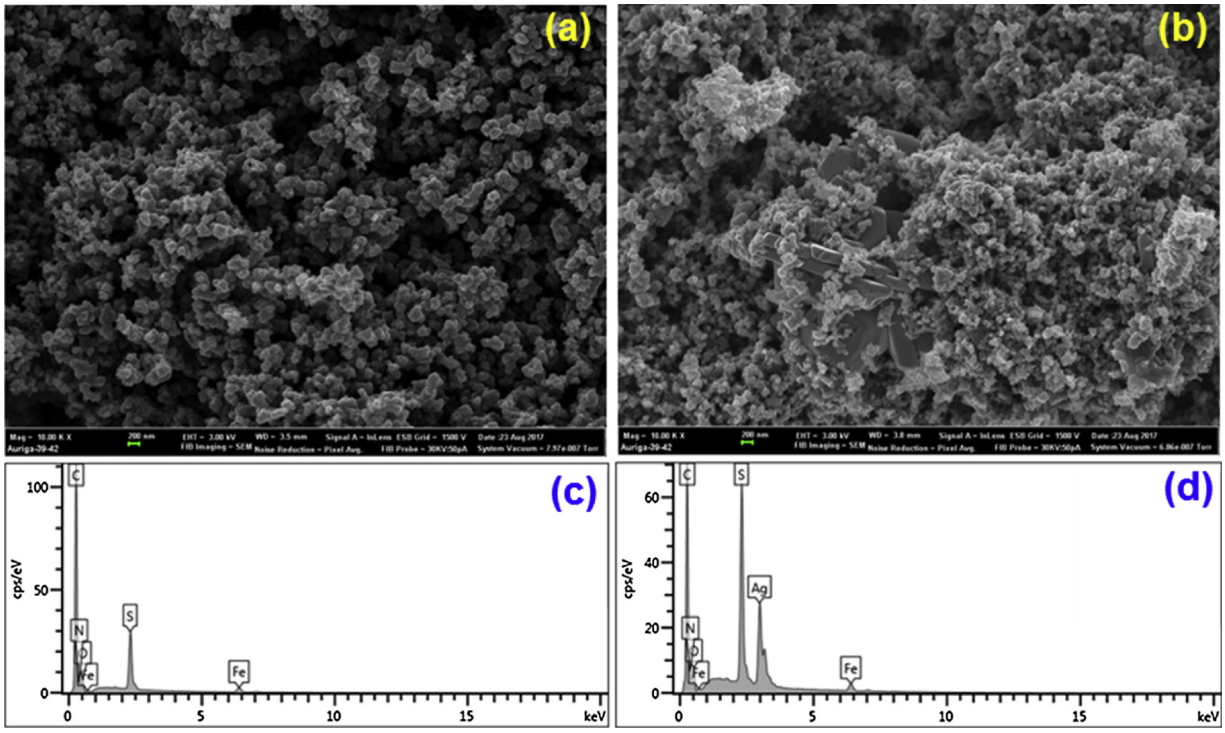

Fig. 1. FE-SEM images of (a) Fe_3O_4@PPy-MAA, (b) Fe_3O_4@PPy-MAA/Ag and EDX spectra of (c) Fe_3O_4@PPy-MAA, (d) Fe_3O_4@PPy-MAA/Ag.

Fe_3O_4@PPy-MAA and Fe_3O_4@PPy-MAA/Ag magnetic nanocomposites. The structural information of pure Fe_3O_4 nanoparticles could be indexed to a face centred cubic (fcc) structure according to XRD pattern in Fig. 3a. A series of major characteristic peaks at 2θ = 30.2°, 35.6°, 43.3°, 53.7°, 57.3° and 62.8°, consistent with the Miller indices (220), (331), (400), (422), (511) and (440) respectively, are observed [40,41]. Fig. 3a also shows the XRD pattern of Fe_3O_4@PPy-MAA nanocomposite. The displayed pattern matches that of pure Fe_3O_4 nanoparticles, indicating the successful incorporation of crystalline and fcc structured magnetic Fe_3O_4 nanoparticles into the modified PPy matrix. The broad diffraction peak at 2θ = 20.5° denotes the scattering from PPy chain at the interplanar spacing [44]. XRD analysis also confirmed the deposition of silver metal onto Fe_3O_4@PPy-MAA adsorbent, where a new phase was identified with five sharp diffraction peaks at 38.12, 44.30, 64.44, 77.40 and 81.7° 2θ values, corresponding to the (111), (200), (220), (311) and (222) crystalline planes of Ag [38,45].

The magnetic property of the as-prepared Fe_3O_4@PPy-MAA was characterised through VSM at room temperature (Fig. 3b). The hysteresis loops of the Fe_3O_4@PPy-MAA composite is S-shape and reveals a weak ferromagnetic response. The estimated value of saturation magnetization (Ms), remanent magnetization (*Mr*), and thickness of the loop *i.e.* coercivity (Hc) was 2.19 emu/g, 0.32 emu/g and 306 Oe, respectively [46]. On the basis of these VSM results, the synthesised Fe_3O_4@PPy-MAA and its Ag-deposited derivative are set to exhibit ferromagnetic behaviour and could be removed from the reaction medium by applying an external magnetic field.

The BET surface areas and pore sizes of the composites developed were measured through nitrogen adsorption-desorption isotherm techniques and the results are shown in Fig. S2 (Supporting information). The adsorption-desorption of all samples exhibited type-IV isotherm with distinct hysteresis loop of type-H3 according to IUPAC classification [47]. The specific surface area of modified polypyrrole (PPy-MAA) increased from 20.67 to 48.48 m^2/g after the incorporation of Fe_3O_4 nanoparticles. Likewise, average pore size also increased from 15.97 to 19.67 nm. However, deposition of Ag NPs onto Fe_3O_4@PPy-MAA surface led to reduction of both the BET surface area (35.69 m^2/g) and pore diameter (13.48 nm). This is probably ascribed to the simultaneously deposition, growth and stabilization of Ag NPs that are very much reliant on the pore size, distribution and surface area of the solid support.

The surface chemical composition of the Fe_3O_4@PPy-MAA and Fe_3O_4@PPy-MAA/Ag composites was also investigated by X-ray photoelectron spectroscopy (XPS). Fig. 4 displays the full survey scan spectra and high resolution XPS spectra of various elements present in both composites. As shown in Fig. 4a, the survey scans spectra of Fe_3O_4@PPy-MAA reveal clear signals of S 2p, C 1 s, N 1 s and O 1 s at 164, 284, 400 and 530 eV, respectively. The signal for Fe was not easily detected as a result of the very low amount of Fe_3O_4 NPs employed during the synthesis of magnetic nanocomposite. However, high-resolution XPS spectra and EDX spectra analyses demonstrated the presence of Fe. The presence of the 3d state of Ag alongside S 2p, C 1 s, N 1 s and O 1 s in the survey scan of Fe_3O_4@PPy-MAA/Ag confirmed the successful deposition of Ag NPs onto the adsorbent surface (Fe_3O_4@PPy-MAA). The high-resolution XPS spectrum of C 1 s, as shown in Fig. 4b, could be deconvoluted to four peaks due to different chemical state of the C atom inside the nanocomposite. The characteristic peaks located at 284.8, 285.7, 287.4 and 288.8 eV are contributions by carbons in −C−C, -C−N/-C−O, −C═O and O═C–O, respectively [48,49]. From the high-resolution XPS spectrum in Fig. 4c, it can be observed that S 2p splits into to two major peaks $2p^{3/2}$ (163.4 eV) and $2p^{1/2}$ (164.5 eV), corresponding to sulphur of sulphide groups [50]. Additionally, the sulphur attributed to $-C-SO_x$ is witnessed at 168.4 eV. The O 1 s spectrum, on the other hand, can be divided into four major peaks (Fig. 4d) situated at 530.7, 531.8, 532.4 and 533.4 eV and corresponding to oxygen of oxide (O^{2-}), −OH, -C–O and O−C═O, respectively [47,51]. The N 1 s spectrum also showed two deconvoluted peaks (Fig. 4e) with binding energy at 399.8 and 401.2 eV, contributions of −NH− and $–N^+$- [52,53]. Fig. 4f shows the high-resolution XPS spectrum with binding energy of 368.2 and 374.2 eV which correspond to Ag $3d^{5/2}$ and Ag $3d^{3/2}$ valence state of deposited Ag NPs. The spin energy separation of 6.0 eV is representative of the metallic silver (Ag°) [54,55]. The Fe 2p high-resolution XPS spectrum of Fe_3O_4@PPy-MAA (Fig. 4g(i)) displayed two weak characteristic peak at 711.5 and 724.8 eV due to Fe $2p^{3/2}$ and Fe $2p^{1/2}$, respectively [56]. Furthermore,

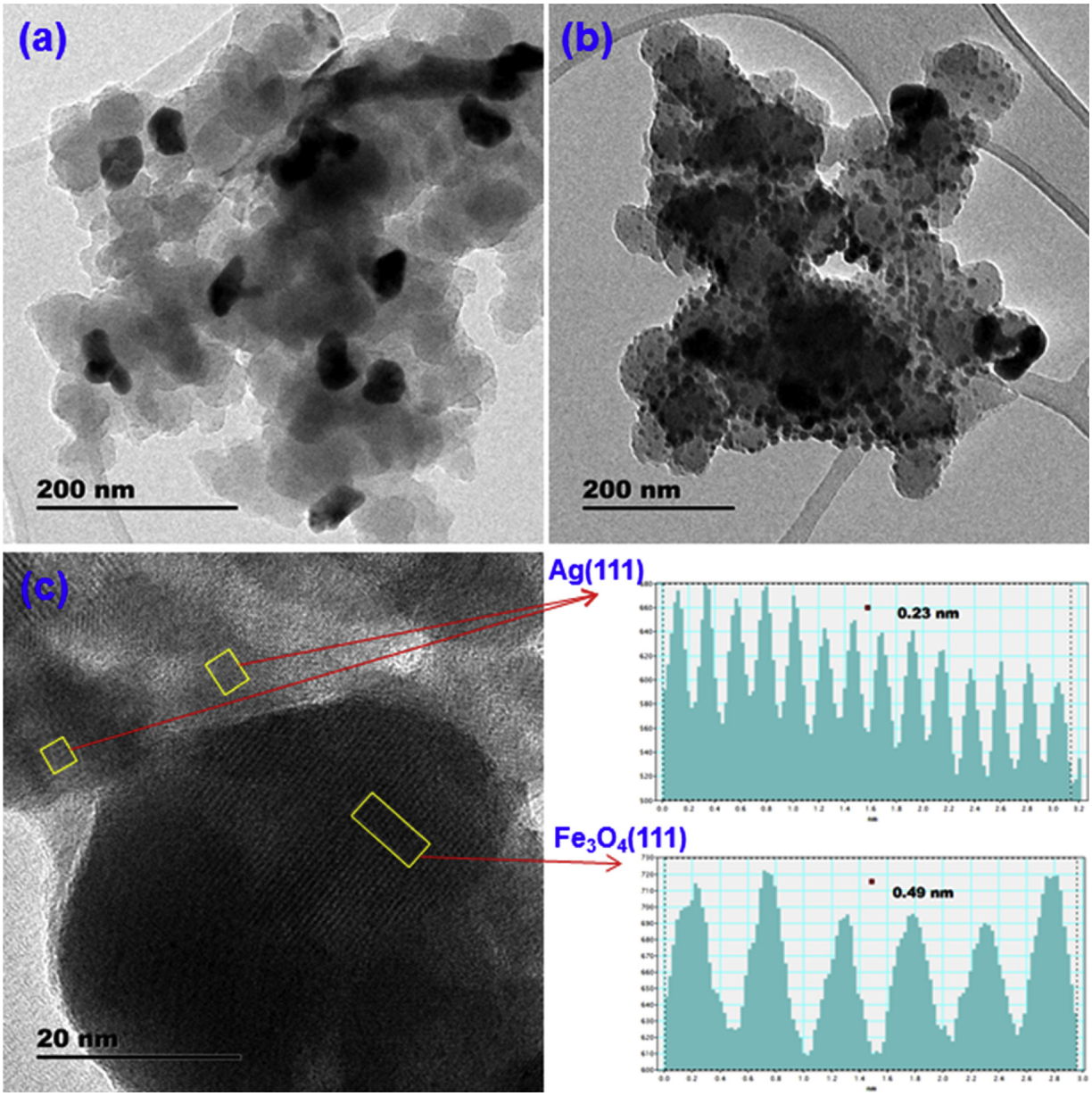

Fig. 2. TEM images of (a) Fe_3O_4@PPy-MAA, (b) Fe_3O_4@PPy-MAA/Ag, (c) HR-TEM displaying the lattice fringes and d spacing of silver and iron nanoparticle.

the Fe_3O_4@PPy-MAA/Ag nanocomposite showed an additional sharp peak corresponding to Ag 3 s in between the binding energy range of Fe $2p^{3/2}$ and Fe $2p^{1/2}$.

3.2. Catalytic reduction of 4-Nitrophenol

To evaluate the catalytic activity of the prepared Fe_3O_4@PPy-MAA/Ag nanocomposite, the reduction of 4-NP has been chosen as a model reaction in the presence of excess $NaBH_4$. The reduction experiments were studied at 25 °C using different amount of catalyst dosage (1.0 to 7.5 mg), 25 mL of 1 mmol aqueous 4-NP solution and 2.5 mL of freshly prepared 1×10^{-1} M $NaBH_4$. The progress of the catalytic reduction was monitored by the UV–vis absorption spectroscopy. During experiment, after addition of freshly prepared $NaBH_4$ solution the maximum UV absorption of the aqueous solution of 4-NP shifted with higher intensity from 318 to 400 nm. The initial colour change (light to intense yellow) associated with red shift after addition of the $NaBH_4$ solution is certainly attributed to the formation of 4-nitrophenolate ions with more pronounced π-conjugated donor-acceptor property [24]. Interestingly, the UV absorption peak of 4-NP at 400 nm and bright yellow colour disappeared with the addition of Fe_3O_4@PPy-MAA/Ag catalyst, after an interval. The progress of the reaction is further confirmed by the appearance and gradual increase in the intensity of a new peak at 300 nm, due to the formation of 4-AP. Fig. 5 represents the absorption spectra of 4-NP *vs* time using 1.0, 2.5, 5.0 and 7.5 mg of Fe_3O_4@PPy-MAA/Ag catalyst. It is clear that with increasing amount of catalyst in the reaction medium, the time required for the conversion of 4-NP to 4-AP decreased. In the presence of 2.5 mg Fe_3O_4@PPy-MAA/Ag, nearly complete reduction of 4-NP was achieved within 45 min with a concomitant change in colour from bright yellow to colourless (Fig. 5a). Under the same reaction conditions (25 mL of 1 mmol 4-NP aqueous solution at 25 °C), but using 5.0 and 7.5 mg of silver loaded catalyst, the time required for the transformation of 4-NP to 4-AP was found to be 35 and 25 min, respectively (Fig. 5b and c). However, at lower catalyst concentration (1.0 mg/25 mL), the reaction was not completed after 90 min (Fig. 5d).

The linear correlation between $\ln(A_t/A_0)$ and reaction time (t) under diverse operation procedure is shown in Fig. S3 (Supporting

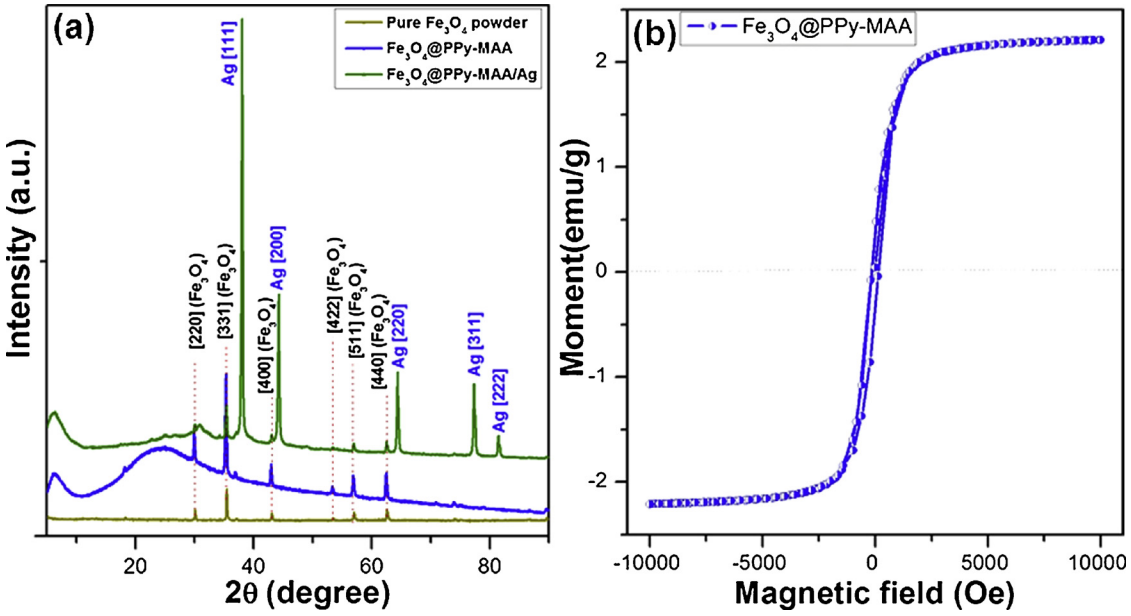

Fig. 3. (a) XRD patterns of Fe_3O_4 powder, Fe_3O_4@PPy-MAA, and Fe_3O_4@PPy-MAA/Ag, (b) Magnetization curves (M–H curves) of Fe_3O_4@PPy-MAA composite.

information). Without the use of the catalyst and in the presence of $NaBH_4$, the absorption peak of 4-NP at 400 nm remains almost unaltered after 180 min. Likewise, when performed in the presence of catalyst and without $NaBH_4$ as reducing agent, the progress of 4-NP reduction was very slow. These events indicate that the presence of both the catalyst and reducing agent ($NaBH_4$) are critical for the development of the reaction. The Fe_3O_4@PPy-MAA adsorbent was also tested for possible catalytic activity in the presence and absence of $NaBH_4$ under similar conditions as described for Fe_3O_4@PPy-MAA/Ag. However, the absorption peak intensity at 400 nm remained nearly

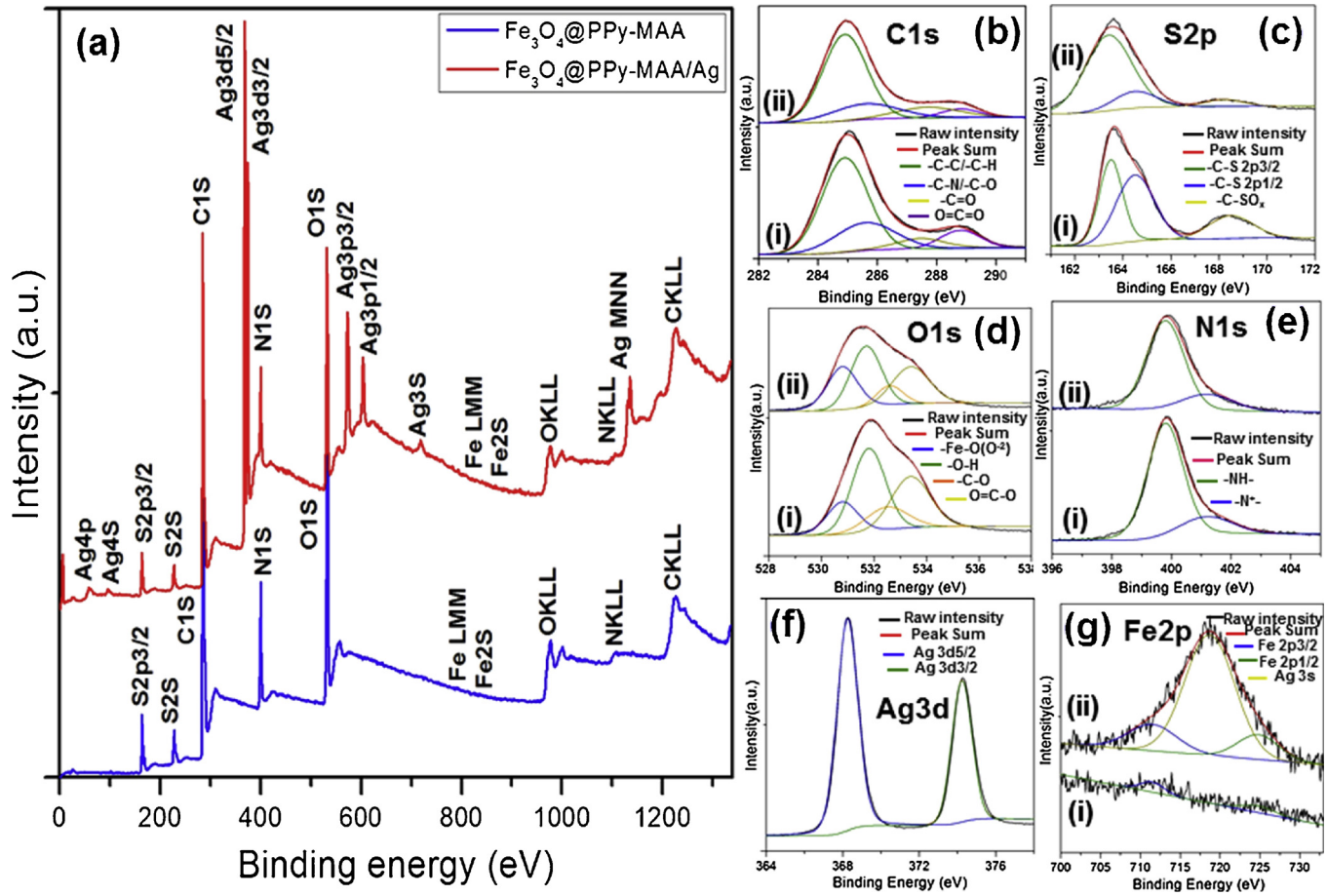

Fig. 4. (a) XPS total spectral survey of Fe_3O_4@PPy-MAA, and Fe_3O_4@PPy-MAA/Ag; high resolution spectra of (b) C 1 s (c) S 2p, (d) O 1 s, (e) N 1 s, (f) Ag 3d and (g) Fe 2p of (i) Fe_3O_4@PPy-MAA, (ii) Fe_3O_4@PPy-MAA/Ag, respectively.

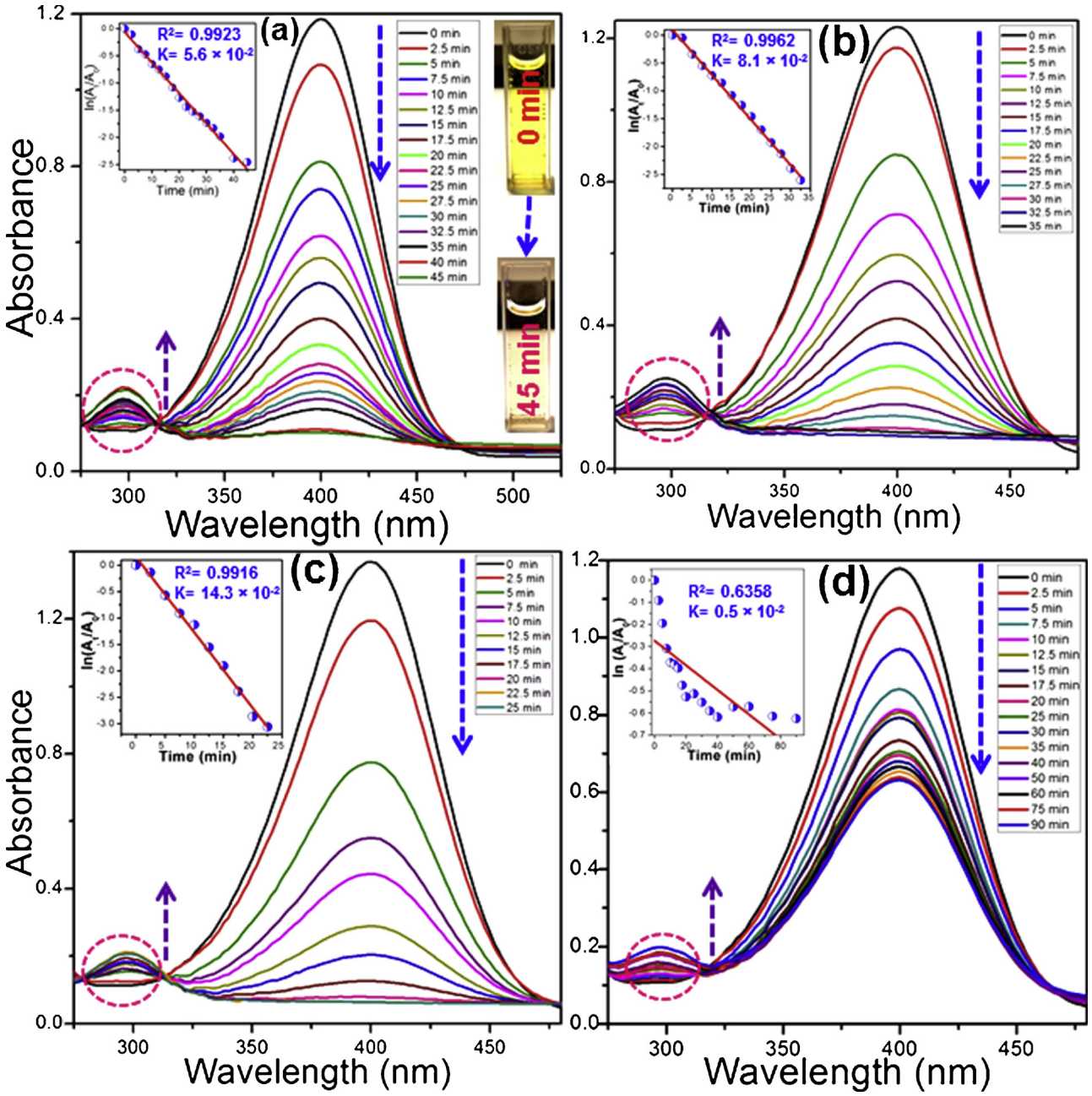

Fig. 5. Time dependent UV–vis spectra for the reduction of 4-nitrophenol and inset shows the plot of $\ln(A_t/A_0)$ vs time in presence of different amount of catalyst (a) 2.5 mg, (b) 5.0 mg, (c) 7.5 mg and (d) 1 mg.

unchanged relative to that of initial 4-NP after 180 min reaction time, indicating that Ag NPs played a key role in -NO_2 transformation.

As excess amount of $NaBH_4$ was employed for the catalytic reduction of 4-NP, the pseudo-first-order kinetics can be considered as a most appropriate equation to evaluate the rate constant of the reaction [57,58]. The apparent rate coefficients were obtained using the following equation:

$$\ln\frac{C_t}{C_0} = \ln\frac{A_t}{A_0} = -kt \quad (1)$$

where C_0 and C_t are the concentration of 4-NP at time t = 0 and t = t, values related to the absorbance of 4-NP, A_0 and A_t, respectively. The rate of the reaction were quantitatively determined from the slopes of the linear plots of $\ln(A_t/A_0)$ against time (t), as shown in Fig. 5(a–d) inset. It is obvious that the inset of Fig. 5(a–c) shows strong linear correlation for the catalytic reduction of 4-NP using 2.5, 5.0 and 7.5 mg of Fe_3O_4@PPy-MAA/Ag catalyst. Moreover, increased mass of catalyst led to improved reduction rate. The estimated pseudo-first-order rate constants were 0.5×10^{-2}, 5.6×10^{-2}, 8.1×10^{-2} and $14.3 \times 10^{-2}\,min^{-1}$ for the reduction of 4-NP using 1.0, 2.5, 5.0 and 7.5 mg of Fe_3O_4@PPy-MAA/Ag nanocomposite, respectively (Table S1; Supporting Information).

Furthermore, aiming at examining the effects of Ag-loading for the catalytic reduction of 4-NP, four different Ag-loaded catalysts (Ag mass loadings: 8.9, 16.5, 36.1 and 42.5 wt%), obtained using silver ion concentrations of 50, 100, 300 and 400 mg/L, respectively, were also probed. Figs. S4 and S5 (Supporting Information) display the UV–vis absorption spectra and plot of $\ln(A_t/A_0)$ *versus* time 't' for the reduction of 4-NP using 7.5 mg of different Ag-loaded catalysts. The nearly complete reduction of 4-NP by Fe_3O_4@PPy-MAA/Ag 8.9, 16.5, 28.3, 36.1 and 42.5 wt% occurred after 45, 35, 25, ~20 and 20 min exposure times, respectively. Moreover, the rate constant values were found to

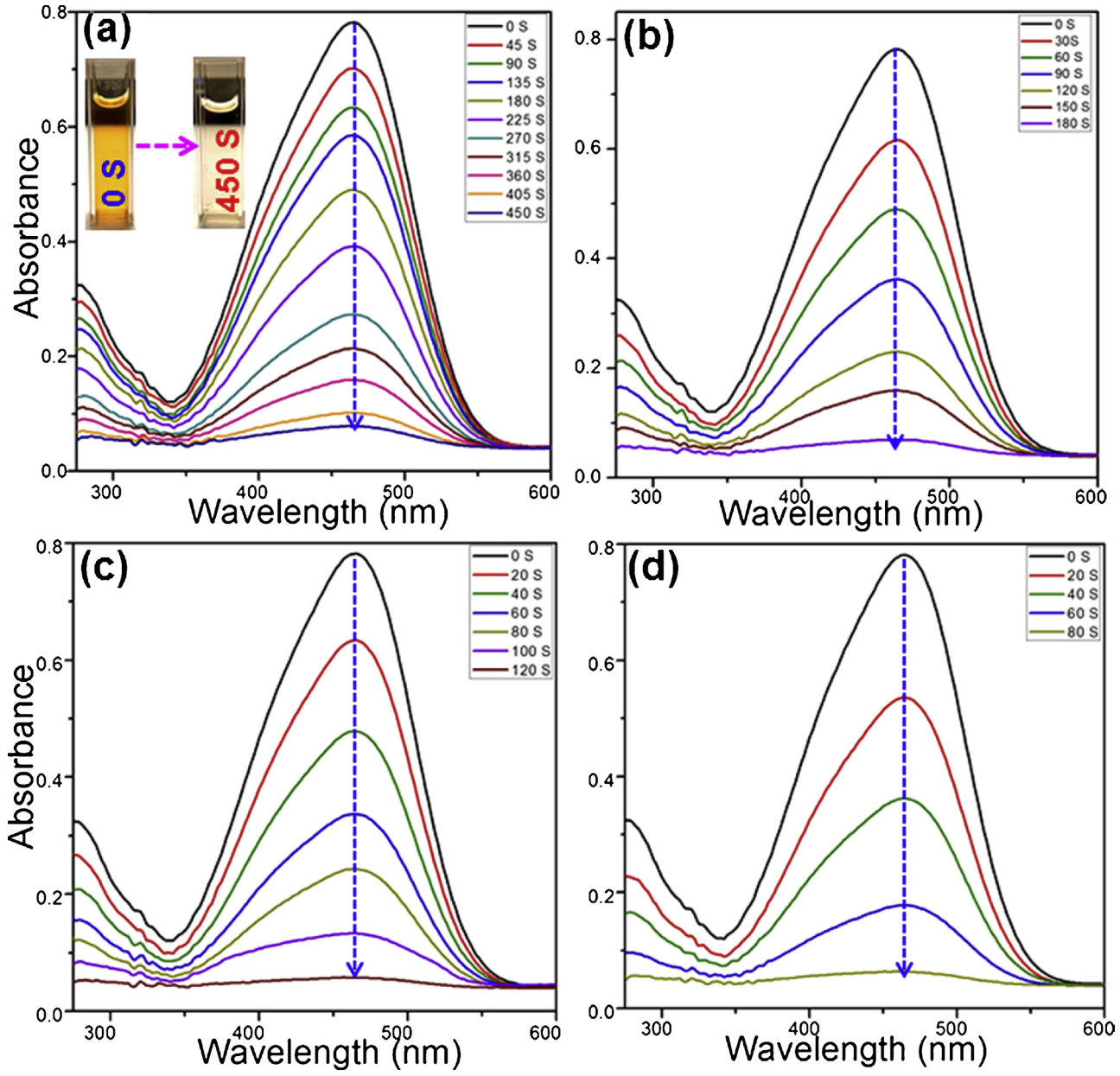

Fig. 6. UV–vis absorption spectral changes for the reduction of MO dye by $NaBH_4$ at various time intervals in the presence of (a) 1.0 mg (b) 2.0 mg, (c) 4.0 mg and (d) 5.0 mg Fe_3O_4@PPy-MAA/Ag catalyst.

increase with increasing Ag mass loading, as shown in Table S1. In the current study, the reduction rate of 4-NP by Fe_3O_4@PPy-MAA/Ag increased substantially with the Ag mass loadings. However, the relatively high content of Ag-loading (40%) could lead to secondary pollution through leaching of Ag from spent catalysts [59].

In an attempt to analyse the reaction mixture for the reduction of 4-NP to 4-AP using Fe_3O_4@PPy-MAA/Ag in the presence of $NaBH_4$ reductant, UPLC-QTOF-MS technique was also utilized. However, the engendered 4-AP, after complete disappearance of 4-NP peak (retention time 2.76 min) could not be detected in both positive (ESI+) and negative (ESI-) modes (Fig. S6; Supporting Information). This finding was ascribed to the poor ionization of 4-AP due to the interfering concentrations of excess sodium borohydride which would prevent stable electro spray ionization through the gas evolution. This issue was encountered previously by Kong et. al. [60] who had to resort to paper assisted ultrasonic spray ionization mass spectrometry (PAUSI-MS) technique.

3.3. Removal of methyl orange (MO) via catalytic reduction and degradation process

Given the excellent catalytic behaviour of Fe_3O_4@PPy-MAA/Ag nanocomposite for the reduction of 4-NP, our next target was to examine its performance in the degradation of hazardous organic dyes. Methyl orange (MO) was chosen initially as a model organic dye, with $NaBH_4$ as a reducing agent. The progress of the MO catalytic degradation process was assessed by monitoring the change in intensity of the UV absorption peak at λ_{max} = 464 nm [36,61]. The time-dependent change in the deep orange colour of the solution, concomitant with the modification in the absorption spectrum of MO is shown in Fig. 6(a–d). The complete decolourization of the MO dye solutions occurred within 450 to 80 s with increasing amount of Fe_3O_4@PPy-MAA/Ag dose (1.0 to 5.0 mg). The rate constants (k) for the degradation of MO dye using different operation procedure were also derived from the pseudo-first-order kinetics. From the linear graphs of $\ln(A_t/A_0)$ *vs* degradation time (Fig. 7(a–d)), the rate constant was 0.52×10^{-2} s^{-1} when using 1.0 mg

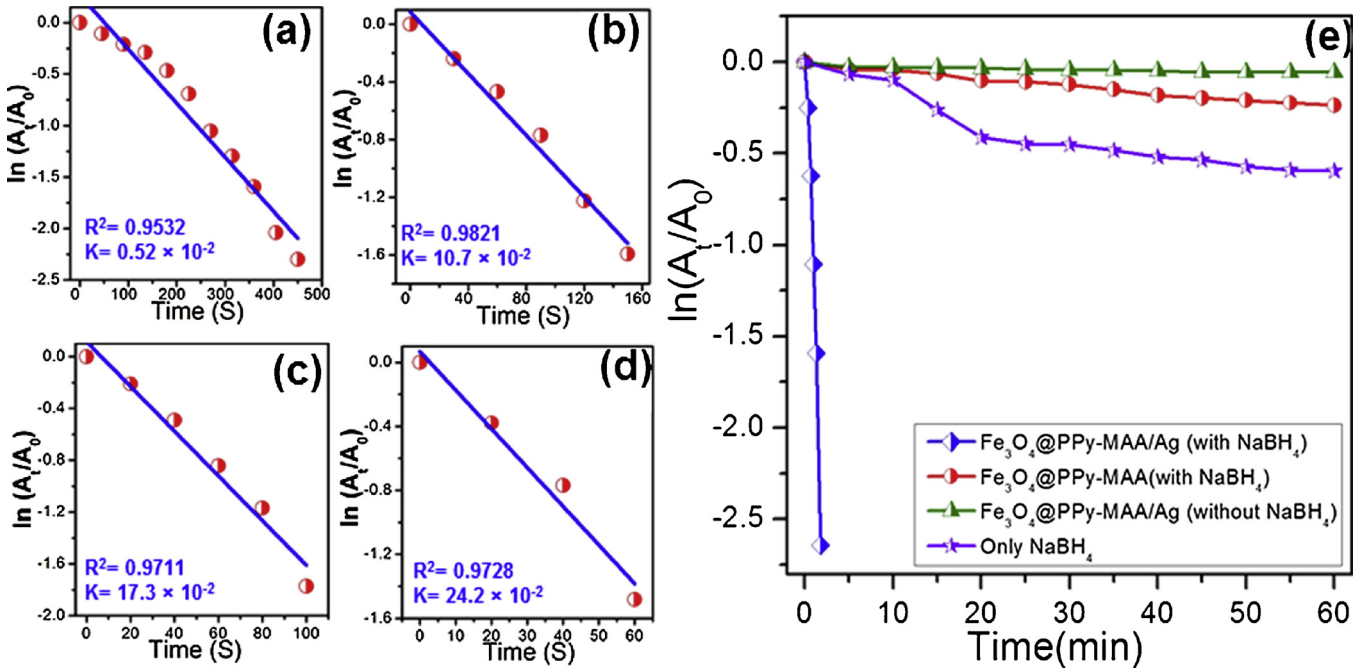

Fig. 7. $\ln(A_t/A_0)$ *versus* reaction time for reduction of MO in presence of Fe_3O_4@PPy MAA/Ag catalyst a) 1.0 mg (b) 2.0 mg, (c) 4.0 mg and (d) 5.0 mg; (e) Kinetics result for the reduction of MO in different catalytic reaction conditions.

catalyst dosage. However, the estimated rate constant values were 10.7×10^{-2}, 17.3×10^{-2} and 24.2×10^{-2} s^{-1} for the degradation study of MO when exposed to 2.0, 4.0 and 5.0 mg Fe_3O_4@PPy-MAA/Ag nanocomposite, respectively. The decrease in MO dye concentration was also monitored using UPLC-QTOF-MS technique. In this case, the rate constant obtained from the residual concentrations of MO was found to be 18.4×10^{-2} s^{-1} under the following conditions: 4. 0 mg of Fe_3O_4@PPy-MAA/Ag, 25 mL aqueous MO solution (1×10^{-4} M) and 1 mL $NaBH_4$ solution (1×10^{-1} M) at 25 °C (Fig. S7). This value compares to that obtained by UV–vis spectroscopic technique (17.3×10^{-2} s^{-1}).

To gain insight into the catalytic efficiency of Fe_3O_4@PPy-MAA/Ag, a correlation study variation of $\ln(A_t/A_0)$ over a time period of 60 min was carried out by altering both the catalyst and reducing agent. Negligible degradation of MO was experienced in the absence of the reductant, as represented in Fig. 7e (green line). However, in the presence of the latter, but with no Ag NPs onto the catalyst, very slow MO degradation was observed after 60 min, as revealed by the red plot. Likewise, the use of $NaBH_4$ only did not achieve significant MO degradation, in contrast to that observed in the presence of Ag-deposited on Fe_3O_4@PPy-MAA nanocomposite and $NaBH_4$. This strongly supports the significant catalytic effect that Ag NPs on the surface Fe3O4@PPy-MAA/Ag nanocomposite have on the degradation of MO dye.

3.4. Catalytic reduction of methylene blue (MB)

The catalytic efficiency of the Ag-deposited nanocomposite was also tested using methylene blue (MB) in aqueous solution. For this study, 25 mL of 1×10^{-4} M MB solution was treated with the prepared catalyst and reducing agent ($NaBH_4$). The change in UV–vis absorption maximum at λ_{max} = 664 nm was employed to monitor the entire reduction process. Fig. 8 displays a series of UV–vis absorption spectra at various intervals time (s), reflecting the degradation of MB using different amounts of Fe_3O_4@PPy-MAA/Ag catalyst. As the reduction progressed, the characteristic peak intensity (λ_{max} = 664 nm) was found to drop markedly and nearly disappeared within 4 min. Fig. 8(a–d) indicates that less time (s) was required for complete disappearance of the intense blue colour (MB) to colourless leucomethylene blue (LMB) when using higher amount of catalyst [62,63]. Loadings of 1.0, 2.0, 4.0 and 5.0 mg Fe_3O_4@PPy-MAA/Ag catalysts effect the complete decolourization within 240, 165, 120 and 90 s, respectively. The rate constants of the reduction kinetics were also calculated from the linear plot of $\ln(A_t/A_0)$ *vs* reduction time (t), and these are presented in the inset of Fig. 8(a–d). These values were 10.1×10^{-3}, 15.7×10^{-3}, 30.8×10^{-3} and 46.8×10^{-3} s^{-1} for the MB reduction using 1.0, 2.0, 4.0 and 5.0 mg of catalyst, respectively. Moreover, the reduction of MB was found to proceed in a similar manner to that of MO, when varying both the catalyst and reductant, as shown in the correlation of $\ln(A_t/A_0)$ against reduction time (Fig. S8, Supporting Information). After 60 min exposure time, there was no major change in the characteristic absorption peak of MB in the absence of either catalyst or reductant. A plausible catalytic reduction pathway is discussed in the following section.

3.5. Reduction mechanism of organic pollutant (4-NP, MO and MB)

The intrinsic hydrolysis of borohydride ions for *4-NP, MO and MB* reduction was investigated using two type of solvents (polar aprotic and polar protic). The reaction of 4-NP with $NaBH_4$ in the presence of Fe_3O_4@PPy-MAA/Ag in DMSO or THF led to only 4% conversion after 2 h. In contrast, the use of EtOH resulted in 41% formation of 4-AP under similar reaction conditions. In the case of MO dye 8 and 47% decolourization was observed in DMSO and EtOH, respectively. Based on the above experimental results a possible mechanism for the reduction of 4-NP and organic dyes using the Fe_3O_4@PPy-MAA/Ag catalyst in the presence of $NaBH_4$ is shown in Scheme 1. The experimental results also show that the reduction rate in the presence of $NaBH_4$ alone is very slow, but accelerated significantly in the presence of Ag metal on the catalyst surface.

In aqueous solution, the hydrolysis of borohydride ions takes place to generate H_2 gas and BO_2^- as shown in Scheme 1 [64]. For 4-NP reduction, the former is adsorbed onto the surface of Ag NPs, leading to formation of a silver hydride complex as hydrogen-mediator. With respect to dye reduction, Ag NPs act as a redox catalyst through electron relay between donor species (BO_2^-) and acceptor molecules (MO or MB) [65,66]. Remarkably, in the case of MB experiment, the colourless

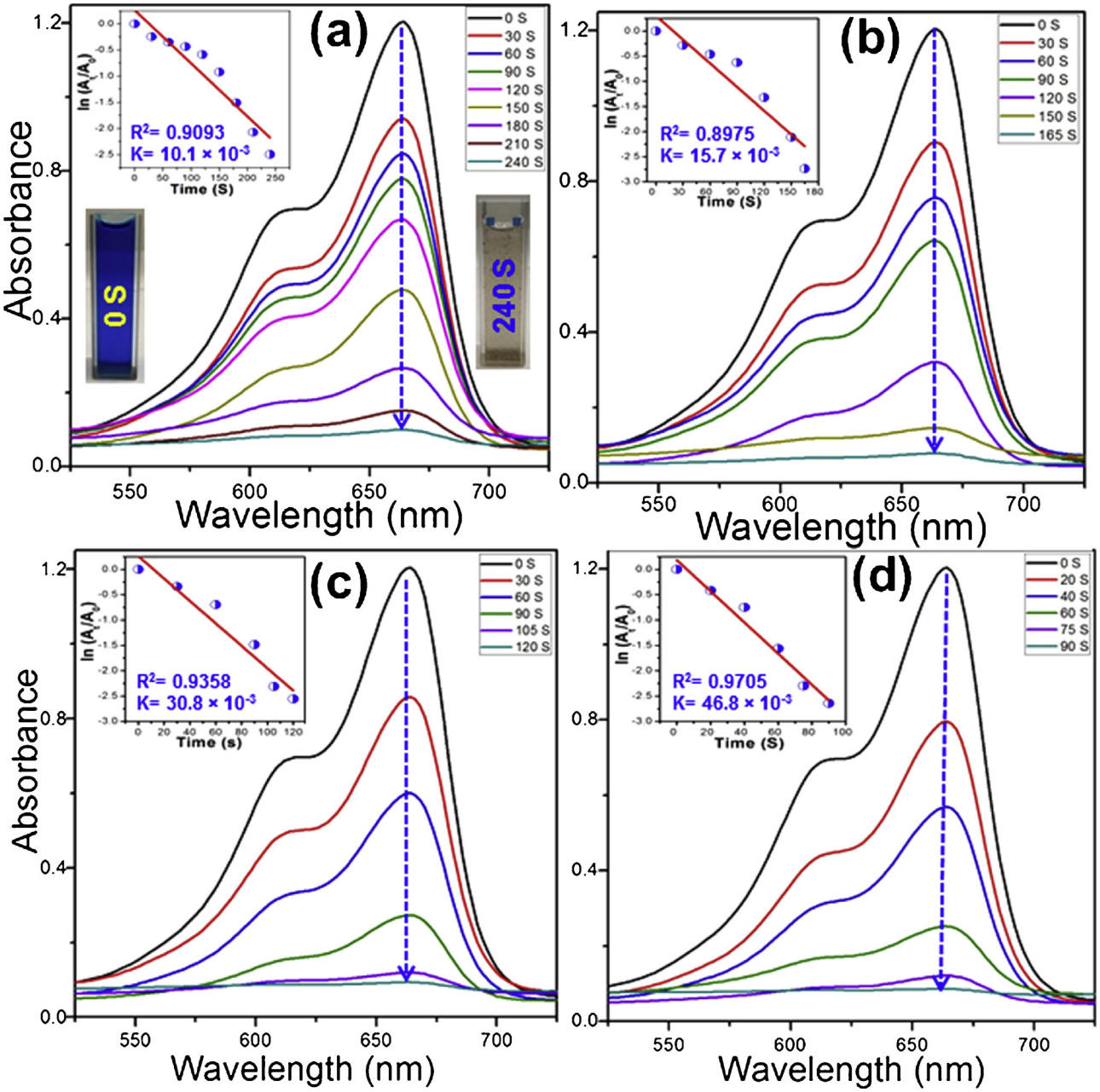

Fig. 8. Time dependent UV–vis spectra for the reduction of MB with the amount of (a) 1.0 mg (b) 2.0 mg, (c) 4.0 mg and (d) 5.0 mg catalyst. Inset shows the corresponding plot of $\ln(A_t/A_0)$ vs reaction time (t).

(reduced) form of MB (LMB) was observed to undergo slow aerial oxidation in open atmosphere after 3–4 hour. However, the characteristic blue colour disappeared upon shacking, as it was once again reduced by the excess $NaBH_4$ present in solution. A Similar observation has been reported previously, and referred as 'clock' reaction [67]. In contrast, the reduced MO solution did not change colour even after several days, revealing that no subsequent re-oxidation process had taken place.

The degraded products of MO dye were analysed using UPLC-QTOF-MS. UPLC chromatograms of untreated MO (time 0 min) and degraded sample for 2 min in electrospray ESI + and ESI- modes, are displayed in Figs. 9a and b. In both ESI + and ESI-, two peaks were detected after 2 min of catalytic degradation using Fe_3O_4@PPy-MAA/Ag and no peak at the retention time corresponding for the untreated MO standard in the UPLC chromatogram. In the ESI- mode, the MO (retention time 4.46 min) was characterized by an *m/z* 304.0758 $[M\text{-}Na]^-$ corresponding to $C_{14}H_{14}N_3O_3S$- (calculated 304.0756). N,*N*-dimethyl-benzene-1,4-diamine (retention time 0.65 min in ESI+) was identified as a breakdown product of MO based on its *m/z* 136.0997 $[M]^-$ corresponding to molecular formula $C_8H_{12}N_2O_3$ (calculated 136.1000) (Fig. 9e) based on the cleavage of the azo bond, responsible for the absorbance in the visible region at 464 nm. The ESI- mode also had a peak at retention time 0.64 min which was identified as 4-amino-benzenesulfonate based on its *m/z* 172.0071 [M]- corresponding to molecular formula $C_6H_6NO_3S$- (calculated 172.0068) (Fig. 9f). Further, the mass spectrograms of degraded MO after 5 min did not show any change relative to that after 2 min. Hence, the MO decolourization products were N,*N*-dimethyl-benzene-1,4-diamine and 4-amino-benzenesulfonate, formed through hydrogenation and subsequently −N-H−NH− bond dissociation as shown in Scheme 1 [68].

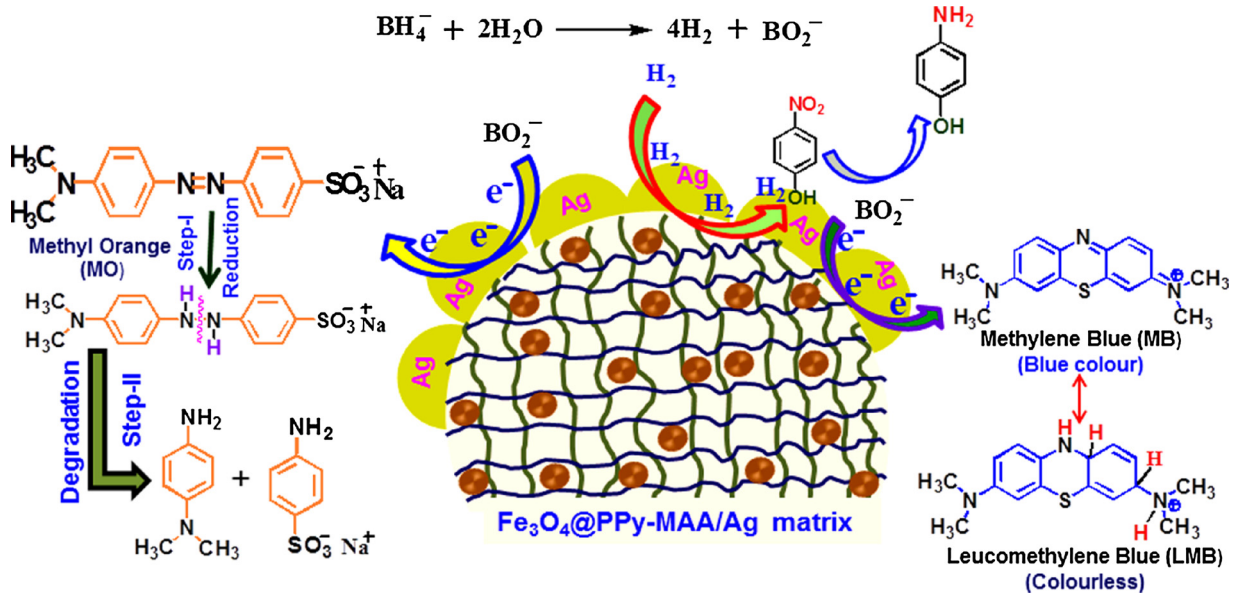

Scheme 1. Plausible mechanism for the reduction of 4-nitrophenol and organic dyes (MO and MB) by Fe_3O_4@PPy-MAA/Ag nanocatalyst.

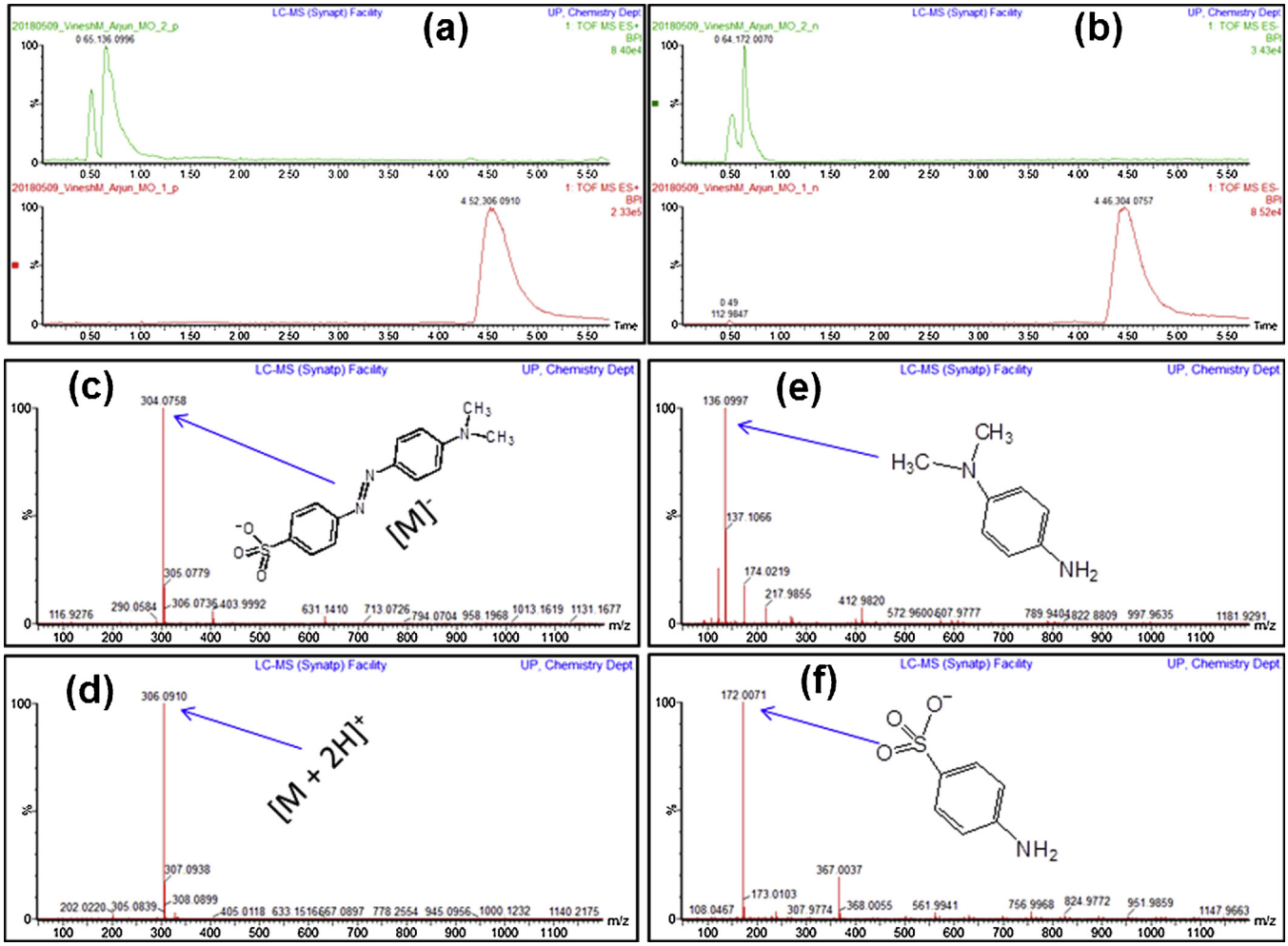

Fig. 9. LC–MS spectra of pure MO and degradation products in (a) positive (b) negative modes. Mass spectra of MO in two different modes (c) and (d); Mass spectra of two degradation products (e) N,*N*-dimethyl-benzene-1,4-diamine and (f) 4-amino-benzenesulfonate.

3.6. Reusability of the catalyst

From the viewpoint of its use in practical applications, it is important to elucidate the reusability of the magnetic nanocatalyst developed, and for this reason the reduction of 4-NP was chosen as model system. Owing to its inherent magnetism, the catalyst was

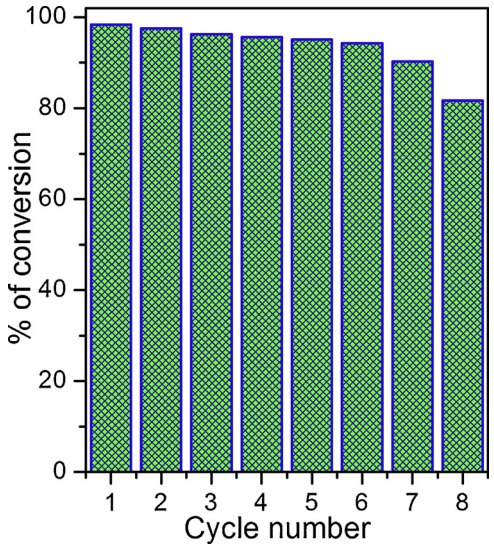

Fig. 10. Reusability of Fe_3O_4@PPy-MAA/Ag nanocatalyst over eight successive cycles for reduction of 4-NP.

separated easily from the reaction mixture with a magnet after the reduction of 4-NP, and washed five times with distilled water before reusing in further recycling. As shown in Fig. 10, the Fe_3O_4@PPy-MAA/Ag was successfully reused in eight successive cycles of 30 min reaction time each. It was noticed that after seven cycles, the catalyst had not exhibited any significant loss of activity. Additionally, more than 80% conversion of 4-NP to 4-AP was achieved after eight successive cycles using the Fe_3O_4@PPy-MAA/Ag nanocomposite. This indicates that the nanocatalyst developed in the current study exhibits excellent stability as well as robustness towards multiple cycles of reuse.

4. Conclusions

A magnetic polypyrrole nanocomposite decorated with Ag NPs (Fe_3O_4@PPy-MAA/Ag) without addition of any reducing agent or stabilizer was successfully synthesized using a simple room temperature protocol. In this green synthesis method, the conducting polymer matrix (Fe_3O_4@PPy-MAA) played an important role for both the reduction of Ag + precursor and stabilization of newly developed Ag NPs on the polymer surface. The formation of Ag NPs on the polymer surface was confirmed by XRD and XPS analyses. It was also confirmed by HR-TEM and FE-SEM studies that Ag NPs were embedded and nicely decorated on the surface of the magnetic nanocomposite. The as-prepared nanocatalyst exhibited excellent catalytic activity towards the reduction of 4-NP to 4-AP in the presence of $NaBH_4$, with reaction rate constants of $0.5–14.3 \times 10^{-2}\,min^{-1}$. In addition, the Fe_3O_4@PPy-MAA/Ag nanocomposite appeared to be a promising catalyst for quick reduction and decolourization of toxic organic dyes (MO and MB) within few minutes (1.0–7.5) using very low catalyst amount (1–5 mg). Kinetic studies revealed that the rate constant of the catalytic reactions improved with increased catalyst dose. The hydrolysis of borohydride ions afforded H_2 gas and the electron rich BO_2^- ions as intermediates for the formation of hydrogen-mediator complex (silver hydride) and electron relay system for the reduction of organic species (4-NP, MO and MB). Therefore, Fe_3O_4@PPy-MAA/Ag is a promising catalyst with potential ability in the reduction of organic toxic pollutants (4-NP, MO and MB) from polluted water bodies.

Acknowledgements

The authors are grateful to the University of Johannesburg, for providing infrastructural facility and financial support. The authors would like to acknowledge National Research Foundation (NRF) and Water Research Commission (WRC), South Africa for financial support. The authors also like to acknowledge the Council for Scientific and Industrial Research (CSIR), and Department of Science and Technology (DST), South Africa, for all their financial contribution to this project along with the characterization unit at the DST-CSIR National Centre for Nanostructured Materials for assisting with materials characterization.

Appendix A. Supplementary data

Supplementary material related to this article can be found, in the online version, at doi:https://doi.org/10.1016/j.apcatb.2018.11.073.

References

[1] F. Mou, J. Guan, H. Ma, L. Xu, W. Shi, ACS Appl. Mater. Interfaces 4 (2012) 3987–3993.
[2] Y.R. Zhang, S.L. Shen, S.Q. Wang, J. Huang, P. Su, Q.R. Wang, B.X. Zhao, Chem. Eng. J. 239 (2014) 250–256.
[3] H. Zhang, D. Chen, X. Lv, Y. Wang, H. Chang, J. Li, Environ. Sci. Technol. 44 (2010) 1107–1111.
[4] Y. Ma, X. Wu, G. Zhang, Appl. Catal. B: Environ. 205 (2017) 262–270.
[5] F.I. Hai, K. Yamamoto, K. Fukushi, Crit. Rev. Environ. Sci. Technol. 37 (2007) 315–377.
[6] C.A. Martınez-Huitle, E. Brillas, Appl. Catal. B: Environ. 87 (2009) 105–145.
[7] A.K. Gupta, A. Pal, C. Sahoo, Dyes Pigm. 69 (2006) 224–232.
[8] M. Mehra, T.R. Sharma, Adv. Appl. Sci. Res. 3 (2012) 849–853.
[9] J. Yang, B. Pan, H. Li, S. Liao, D. Zhang, M. Wu, B. Xing, Environ. Sci. Technol. 50 (2) (2016) 694–700.
[10] S. Yi, W.Q. Zhuang, B. Wu, S.T.L. Tay, J.H. Tay, Environ. Sci. Technol. 40 (2006) 2396–2401.
[11] J. Shen, X. Xu, X. Jiang, C. Hua, L. Zhang, X. Sun, J. Li, Y. Mu, L. Wang, Water Res. 67 (2014) 11–18.
[12] P. Deka, R.C. Deka, P. Bharali, New J. Chem. 38 (2014) 1789–1793.
[13] H. Liu, Z. Bi, X.G. Sun, R.R. Unocic, M.P. Paranthaman, S. Dai, G.M. Brown, Adv. Mater. 23 (2011) 3450–3454.
[14] J. Chang, J. Sun, C. Xu, H. Xu, L. Gao, Nanoscale 4 (2012) 6786–6791.
[15] K. He, G. Chen, G. Zeng, A. Chen, Z. Huang, J. Shi, T. Huang, M. Peng, L. Hu, Appl. Catal. B: Environ. 228 (2018) 19–28.
[16] D. Astruc, F. Lu, J.R. Aranzaes, Angew. Chem. Int. Ed. 44 (2005) 7852–7872.
[17] T. Ji, L. Chen, M. Schmitz, F.S. Bao, J. Zhu, Green Chem. 17 (2015) 2515–2523.
[18] Z. Huanga, G. Chen, G. Zeng, Z. Guo, K. He, L. Hu, J. Wu, L. Zhang, Y. Zhu, Z. Song, J. Hazard. Mater. 321 (2017) 37–46.
[19] Z. Huang, Z. Zeng, A. Chen, G. Zeng, R. Xiao, P. Xu, K. He, Z. Song, L. Hu, M. Peng, T. Huang, G. Chen, Chemosphere 203 (2018) 199–208.
[20] J. He, W. Ji, L. Yao, Y. Wang, B. Khezri, R.D. Webster, H. Chen, Adv. Mater. 26 (2014) 4151–4155.
[21] Y. Dai, W. Zheng, X. Li, B. Chen, L. Wang, G. He, Chem. Eng. J. 293 (2016) 252–258.
[22] W. Yan, B. Chen, S.M. Mahurin, S. Dai, S.H. Overbury, Chem. Commun. 17 (2004) 1918–1919.
[23] J.M. Campelo, D. Luna, R. Luque, J.M. Marinas, A.A. Romero, Chem. Sus. Chem. 2 (2009) 18–45.
[24] Y. Choi, H.S. Bae, E. Seo, S. Jang, K.H. Park, B.S. Kim, J. Mater. Chem. 21 (2011) 15431–15436.
[25] E. Hariprasad, T. Radhakrishnan, ACS Catal. 2 (2012) 1179–1186.
[26] L. Shang, T. Bian, B. Zhang, D. Zhang, L.Z. Wu, C.H. Tung, Y. Yin, T. Zhang, Angew. Chem. 126 (2014) 254–258.
[27] A. Dhakshinamoorthy, H. Garcia, Chem. Soc. Rev. 41 (2012) 5262–5284.
[28] L. Jiwei, Q. Jingxia, Y. Miao, J. Chen, J. Mater. Sci. 43 (2008) 6285–6288.
[29] P.K. Khanna, S. Bhanoth, V. Dhanwe, A. Kshirsagar, P. More, RSC Adv. 5 (2015) 92818–92828.
[30] V. Selvaraj, M. Alagar, K.S. Kumar, Appl. Catal. B: Environ. 75 (2009) 129–138.
[31] A. Chen, K. Kamata, M. Nakagawa, T. Iyoda, H. Wang, X. Li, J. Phys. Chem. B 109 (2005) 18283–182883.
[32] S.T. Selvan, Chem. Commun. 3 (1998) 351–352.
[33] H. Zhang, X. Zhong, J.J. Xu, H.Y. Chen, Langmuir 24 (2008) 13748–13752.
[34] S.V. Asmussen, C.I. Vallo, Eur. Polym. J. 79 (2016) 163–175.
[35] B. Hu, Y. Zhao, H.Z. Zhu, S.H. Yu, ACS Nano 4 (2011) 3166–3171.
[36] P. Mohammadi, H. Sheibani, Appl. Organometal. Chem. 4 (2018) 4249.
[37] V. Polshettiwar, B. Baruwati, R.S. Varma, Green Chem. 11 (2009) 127–131.
[38] R. Das, S. Giri, A.L.K. Abia, B. Dhonge, A. Maity, ACS Sustain. Chem. Eng. 5 (2017) 2711–2724.
[39] J.M. Hodges, A.J. Biacchi, R.E. Schaak, ACS Nano 8 (2014) 1047–1055.
[40] C. Jin, Y. Qu, M. Wang, J. Han, Y. Hu, R. Guo, Langmuir 32 (2016) 4595–4601.
[41] C. Karunakaran, P. Vinayagamoorthy, J. Jayabharathi, Langmuir 30 (2014) 15031–15039.
[42] A.E. Vikraman, A.R. Jose, M. Jacob, K.G. Kumar, Anal. Methods 7 (2015) 6791–6798.
[43] X. Zhang, J. Zhang, W. Song, Z. Liu, J. Phys. Chem. B 110 (2006) 1158–1165.
[44] N. Ballav, R. Das, S. Giri, A.M. Muliwa, K. Pillaya, A. Arjun Maity, Chem. Eng. J.

345 (2018) 621–630.
[45] Y. Yao, B. Gao, F. Wu, C. Zhang, L. Yang, ACS Appl. Mater. Interfaces 7 (2015) 10634–10640.
[46] L. Xu, J. Du, P. Li, Y. Qian, J. Phys. Chem. B 110 (2006) 3871–3875.
[47] Y. Liu, Y. Jiao, Z. Zhang, F. Qu, A. Umar, X. Wu, ACS Appl. Mater. Interfaces 6 (2014) 2174–2184.
[48] S. Zhang, X.Y. Li, J.P. Chen, J. Colloid Interface Sci. 343 (2010) 232–238.
[49] Z. Geng, Y. Lin, X. Yu, Q. Shen, L. Ma, Z. Li, N. Pan, X. Wang, J. Mater. Chem. 12 (2012) 3527–3535.
[50] J.S. Li, S.L. Li, Y.J. Tang, K. Li, L. Zhou, N. Kong, Y.Q. Lan, J.C. Bao, Z.H. Dai, Sci. Rep. 4 (2014) 5130.
[51] K. Song, Y. Lee, M.R. Jo, K.M. Nam, Y.M. Kang, Nanotechnology 23 (2012) 505401.
[52] S.W. Huang, K.G. Neoh, E.T. Kanga, H.S. Han, K.L. Tan, J. Mater. Chem. 8 (8) (1998) 1743–1748.
[53] Y. Wei, L. Li, X. Yang, G. Pan, G. Yan, X. Yu, Nanoscale Res. Lett. 5 (2010) 433–437.
[54] M. Kumar, S. Deka, ACS Appl. Mater. Interfaces 6 (2014) 16071–16081.
[55] D.H. Yu, X. Yu, C. Wang, X.C. Liu, Y. Xing, ACS Appl. Mater. Interfaces 4 (2012) 2781–2787.
[56] P. Kumar, C. Joshi, A. Barras, B. Sieber, A. Addad, L. Boussekeyd, S. Szunerits, R. Boukherroub, S.L. Jain, Appl. Catal. B: Environ. 205 (2017) 654–665.
[57] P. Veerakumar, P. Muthuselvam, P. Thanasekaran, K.C. Lin, Inorg. Chem. Front. 5 (2018) 354–363.
[58] R. Rajesh, E. Sujanthi, S.S. Kumar, R. Venkatesan, Phys. Chem. Chem. Phys. 17 (2015) 11329–11340.
[59] P.P. Sun, H. Song, T.Y. Kim, B.J. Min, S.Y. Cho, Ind. Eng. Chem. Res. 53 (2014) 20241–20246.
[60] X. Kong, H. Zhu, C.L. Chen, G. Huang, Q. Chen, Chem. Phys. Lett. 684 (2017) 148–152.
[61] R. Rajesh, S.S. Kumar, R. Venkatesan, New J. Chem. 38 (2014) 1551–1558.
[62] P. Veerakumar, S.M. Chen, R. Madhu, V. Veeramani, C.T. Hung, S.B. Liu, ACS Appl. Mater. Interfaces 7 (2015) 24810–24821.
[63] A. Mignani, S. Fazzini, B. Ballarin, E. Boanini, M.C. Cassani, C. Maccato, D. Barreca, D. Nanni, RSC Adv. 5 (2015) 9600–9606.
[64] S. Carregal-Romero, J. Pérez-Juste, Pablo Hervés, L.M. Liz-Marzán, P. Mulvaney, Langmuir 26 (2) (2010) 1271–1277.
[65] K. Mallick, M. Witcomb, M. Scurrell, Mater. Chem. Phys. 97 (2006) 283–287.
[66] A. Nautiyal, S.R. Shukla, J. Water Process Eng. 22 (2018) 276–285.
[67] S. Pande, S. Jana, S. Basu, A.K. Sinha, A. Datta, T. Pal, J. Phys. Chem. C 112 (2008) 3619–3626.
[68] Z. Jia, H. Sun, Z. Du, Z. Lei, J. Environ. Sci. China 26 (2) (2014) 478–482.